Quantum enhancement of a single quantum battery by repeated interactions with large spins

P. Chen⊙, T. S. Yin⊙, Z. Q. Jiang,* and G. R. Jin†

Physics Department of Zhejiang Sci-Tech University, Hangzhou 310018, China

A generalized collision model is developed to investigate coherent charging a single quantum battery by repeated interactions with many-atom large spins, where collective atom operators are adopted and the battery is modeled by a uniform energy ladder. For an initially empty battery, we derive analytical results of the average number of excitations and hence the charging power in the short-time limit. Our analytical results show that a faster charging and an increased amount of the power in the coherent protocol uniquely arise from the phase coherence of the atoms. Finally, we show that the charging power defined by the so-called ergotropy almost follows our analytical result, due to a nearly pure state of the battery in the short-time limit.

I. INTRODUCTION

One of the central goals of quantum thermodynamics is to improve the thermodynamic processes via quantum resources and quantum operators [1–5]. The simplest setup to achieve the quantum advantages in the thermodynamics is the so-called quantum batteries (QBs) [6–9], i.e., a small quantum system that stores and provides energy. Starting from seminal ideas developed in Ref. [6], various quantum systems have been considered as the candidate of the QBs, including collective spins [10–12], interacting spin chains [13–15], and mechanical flywheels [16,17]. Different from classical batteries, the QBs explore phase coherence [18] and quantum entanglement [19–23] as useful resources to improve the performance of the QBs. A notable example is the Dicke-model QBs [24–27] based on collective superradiant coupling in cavity and waveguide QED setups, which has been experimentally demonstrated by using fluorescent organic molecules in a microcavity [28].

Recently, the QBs have been realized with a transmon qutrit [29] and a solid-state qubit [30,31], which clearly demonstrate the quantum advantage at the level of a single battery [32–34]. Especially, Seah *et al.* [32] present a collision model to investigate the repeated charging of a single battery by a sequence of identical qubits, where a single two-level qubit is adopted as the charger in each interaction or collision. The collision model describes a system that undergoes successive interactions or collisions with the auxiliary systems [35–38]. It has been used in various research areas, such as non-Markovian quantum dynamics [39], quantum thermodynamics [40,41], quantum optics [42], and quantum gravity [43]. Using the collision model, Seah *et al.* [32] numerically show that the phase coherence of the qubit can realize a faster charging and a larger amount of the charging power in a comparison with that of the qubit state without any

coherence. To understand the role of the coherence, analytical results of the charging energy and its power are necessary.

In this paper, we generalize the collision model to investigate coherent charging of a single quantum battery by repeated interactions with many two-level atoms (or, equivalently, a large spin), where collective atomic operators $\{\hat{J}_{\pm}, \hat{J}_z\}$ are adopted and the battery is modeled by a uniform energy ladder [32,44]. Analytical results of the charging energy and its power are derived by considering the initially empty battery and the short-time limit of the interaction at each charging step. Following Ref. [32], we compare the charging processes with the atomic coherence $\langle \hat{J}_- \rangle \neq 0$, corresponding to the coherent charging, and $\langle \hat{J}_- \rangle = 0$ for the incoherent charging. Our analytical results show that the advantage of the coherent protocol uniquely comes from the atomic coherence. Furthermore, we show that the amount of the charging power reaches its maximum (proportional to the number of atoms N_A) when all the atoms are prepared in a superposition state, i.e., a coherent spin state $|\theta_0, \phi_0\rangle$ with $\theta_0 = \pi/2$ and $\phi_0 = 0$. Finally, we investigate the charging power defined by the so-called ergotropy [45]. In the short-time limit, numerical results of the power show good agreement with the analytical result, since the battery state almost maintains in a pure state.

II. GENERALIZED COLLISION MODEL FOR THE QUANTUM BATTERY

As illustrated schematically by Fig. 1, we consider a quantum battery $\hat{\rho}_B$ modeled by a uniform energy ladder [32,44], which undergoes successive interactions with identical two-level atoms confined in several lattices. The interaction between the battery and the atoms at each collision can be described by the Hamiltonian

$$\hat{H} = \hat{H}_0 + \hat{V} = \varepsilon\hat{J}_z + \varepsilon\hat{n} + \hbar g(\hat{J}_+\hat{B} + \hat{J}_-\hat{B}^\dagger), \quad (1)$$

where collective atomic operators $\hat{J}_z = \sum_{i=1}^{N_A}(|e\rangle_{ii}\langle e| - |g\rangle_{ii}\langle g|)/2$ and $\hat{J}_+ = \sum_{i=1}^{N_A}|e\rangle_{ii}\langle g| = (\hat{J}_-)^\dagger$ are introduced to describe finite N_A identical atoms, with the ground state $|g\rangle$ and the excited state $|e\rangle$. For the battery, one can define the

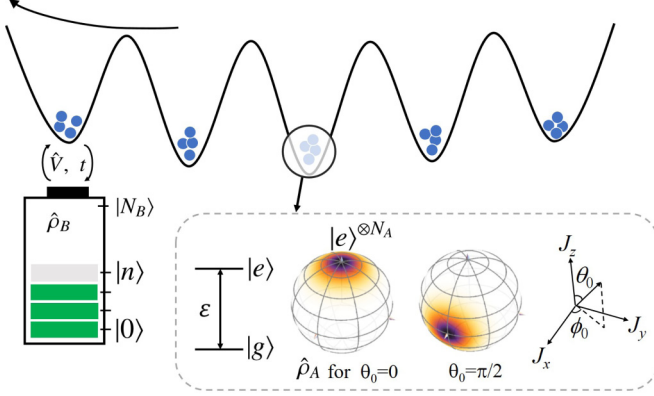*jiangzhongqing@163.com
†grjin@zstu.edu.cn

FIG. 1. Schematic picture of a single battery (modeled by a uniform energy ladder with $N_B + 1$ levels), which undergoes successive interactions with finite N_A two-level atoms confined in each lattice. The optimal atom states $\hat{\rho}_A$ for the incoherent and the coherent charging protocols correspond to the coherent spin states of a large spin $|\theta_0, \phi_0\rangle$, with $\theta_0 = 0, \pi/2$, as illustrated by their quasiprobability distributions on the Bloch sphere.

number operator $\hat{n} = \sum_{n=0}^{N_B} n|n\rangle\langle n|$, where N_B denotes the highest level of the battery, and also the ladder operators

$$\hat{B} = \sum_{n=1}^{N_B} |n-1\rangle\langle n|, \quad \hat{B}^\dagger = \sum_{n=1}^{N_B} |n\rangle\langle n-1|, \quad (2)$$

satisfying the commutation relation [46,47]: $[\hat{B}, \hat{B}^\dagger] = |0\rangle\langle 0| - |N_B\rangle\langle N_B|$. When the occupations of $|0\rangle$ and $|N_B\rangle$ are vanishing, it becomes $[\hat{B}, \hat{B}^\dagger] \approx 0$, corresponding to the no-boundary condition. If we only omit the upper boundary (i.e., the occupation on $|N_B\rangle$ is vanishing), then the commutation relation is simply given by $[\hat{B}, \hat{B}^\dagger] \approx |0\rangle\langle 0|$.

In experiments, the identical atoms (considered here as the charger) can be realized by an ensemble of large spins at the room temperature (e.g., the spin $j = 7/2$ of cesium atoms [48,49]) or ultracold bosonic gases in optical lattice [50–52]. On the other hand, the energy ladder can be realized by a cavity mode with a *finite* number of energy levels [33,34]. In the interaction picture, the Hamiltonian becomes $\hat{V}_{\text{int}} = \exp(i\hat{H}_0 t/\hbar)\hat{V}\exp(-i\hat{H}_0 t/\hbar) = \hat{V}$, due to $[\hat{H}_0, \hat{V}] = 0$, which in turn gives the time evolution operator $\hat{U}_\tau = \exp[-i\tau(\hat{J}_+ \hat{B} + \hat{J}_- \hat{B}^\dagger)]$, where $\tau = gt$ and t denotes the interaction time at each charging step. Starting from an initial state $\hat{\rho}_B(0)$, the battery state at the kth collision becomes

$$\hat{\rho}_B(k) = \text{Tr}_A[\hat{U}_\tau \hat{\rho}_B(k-1) \otimes \hat{\rho}_A \hat{U}_\tau^\dagger], \quad (3)$$

where $\text{Tr}_A(\cdots)$ denotes the trace over the atom states. Similar to Ref. [32], we assume that the atom states are identical for all the collisions (i.e., $\hat{\rho}_A$ is independent on k). In the limit $\tau \to 0$, the time evolution operator can be approximated as $\hat{U}_\tau \approx 1 - i\tau(\hat{J}_+ \hat{B} + \hat{J}_- \hat{B}^\dagger)$, and therefore

$$\hat{\rho}_B(k) \approx \hat{D}^\dagger(k\alpha)\hat{\rho}_B(0)\hat{D}(k\alpha), \quad (4)$$

where $\hat{D}(\alpha) = \exp(\alpha\hat{B}^\dagger - \alpha^*\hat{B})$ and $\alpha = i\tau\langle\hat{J}_-\rangle$, with $\langle(\cdots)\rangle = \text{Tr}_A[\hat{\rho}_A(\cdots)]$. A similar result of Eq. (4) has been obtained by Ref. [34] (see also Appendix A).

Using the probability distribution $P_n(k) = \langle n|\hat{\rho}_B(k)|n\rangle$, one can define the mean number of excitations and the mean

energy [32]:

$$\bar{n}_k = \sum_{n=0}^{N_B} nP_n(k), \quad E(k) = \varepsilon\bar{n}_k, \quad (5)$$

where ε denotes the energy spacing of the battery. Following Ref. [32], we first consider the no-boundary condition (i.e., the occupations on $|0\rangle$ and $|N_B\rangle$ are vanishing), which allows us to obtain a recursion relation (see Appendix A),

$$\bar{n}_k = \bar{n}_{k-1} + v + \text{Im}(\Omega\beta_{k-1}^*), \quad (6)$$

where $v = 2\sin^2(\tau)\langle\hat{J}_z\rangle$, $\Omega = \sin(2\tau)\langle\hat{J}_-\rangle$, and $\beta_k = \text{Tr}_B[\hat{\rho}_B(k)\hat{B}]$. Without any boundary, we have $\beta_k = \beta_0$, and therefore $\bar{n}_k = \bar{n}_0 + k[v + \text{Im}(\Omega\beta_0^*)]$, where Eq. (6) has iterated for k times. One can easily find that the mean number of excitations $\bar{n}_k$ and hence the mean energy of the battery $E(k)$ grow linearly with respect to the number of charging steps k [32]. When $\bar{n}_k \approx N_B$, the battery can be regarded as being fully charged.

Next we focus on the short-time limit (i.e., $\tau \to 0$) to obtain $v \approx 2\tau^2\langle\hat{J}_z\rangle \sim 0$ and $\Omega \approx 2\tau\langle\hat{J}_-\rangle = -2i\alpha$, which yield

$$\bar{n}_k \approx \bar{n}_{k-1} - (\alpha\beta_{k-1}^* + \alpha^*\beta_{k-1}), \quad (7)$$

where the lower boundary $|0\rangle$ has been taken into account (see Appendix B) as

$$\beta_k = \beta_0 - \alpha \sum_{k'=0}^{k-1} \langle 0|\hat{\rho}_B(k')|0\rangle. \quad (8)$$

Note that the above recursion relations of the average number of excitations, i.e., Eqs. (6) and (7), are independent on any specific form of $\hat{\rho}_A$, and even free from the initial state of $\hat{\rho}_B(0)$. Next, we consider a specific form of $\hat{\rho}_A$ and extend the single-particle case (i.e., $N_A = 1$) [32] into the many-particle case, for which the total charging process becomes faster and the amount of charging power can be increased, dependent on N_A.

III. COLLECTIVELY COHERENT CHARGING

In Ref. [32], Seah *et al.* consider the battery charged by a sequence of a single atom (i.e., $N_A = 1$), with the atom state [53–58]

$$\hat{\rho}_A = \cos^2\left(\frac{\theta_0}{2}\right)|e\rangle\langle e| + \sin^2\left(\frac{\theta_0}{2}\right)|g\rangle\langle g|$$

$$+ c\left(\frac{\sin(\theta_0)}{2}e^{-i\phi_0}|e\rangle\langle g| + \text{H.c.}\right), \quad (9)$$

where θ_0 and ϕ_0 determine the population imbalance and the relative phase between the two states [56–58], as shown in Fig. 1. The parameter $c \in [0, 1]$ is added artificially to distinguish the two opposing protocols: the incoherent charging ($c = 0$) and the coherent charging ($c = 1$). The spin-1/2 can be mapped into a large spin system with $j = N_A/2$, for which the atom state becomes

$$\hat{\rho}_A = \sum_m \rho_{m,m}|j, m\rangle\langle j, m| + c\sum_{m\neq m'} \rho_{m,m'}|j, m\rangle\langle j, m'|, \quad (10)$$
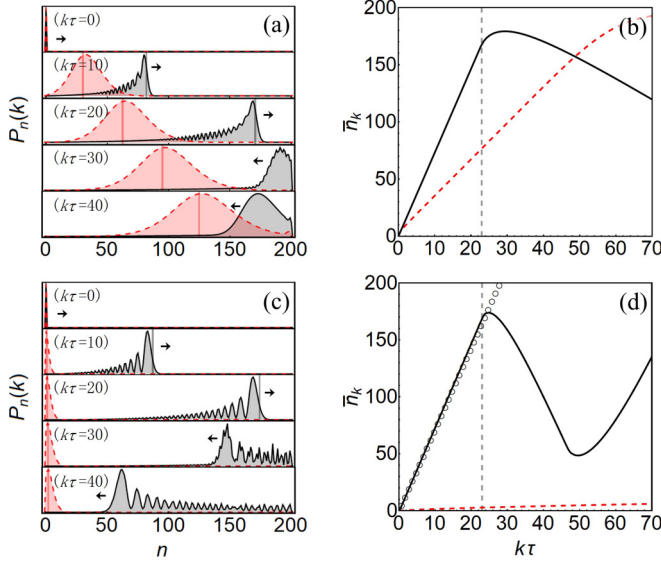
FIG. 2. Probability distributions of $\hat{\rho}_B(k)$ (left panel) and average number of the excitations (right panel), for different values of the charging time $\tau = \pi/4$ [in (a) and (b)] and 0.01 [(c) and (d)]. Solid (red dashed) lines correspond to the coherent (incoherent) charging protocol. All curves in the left panel are rescaled to their associated maxima. Vertical lines: location of the peak $n \approx (v + \Omega)k$ (left panel) and $k_{est}\tau$ (right panel), determined by Eqs. (12) and (13), respectively. Circles in (d): analytical result of $\bar{n}_k$, given by Eq. (17). Parameters: $N_A = 10$, $N_B = 200$, and $\theta_0 = \pi/3$.

where $\{|j, m\rangle\}$ denote eigenstates of $\hat{J}_z$ and $\rho_{m,m'} = d_m d_{m'}^*$, with

$$d_m = \binom{2j}{j+m}^{1/2} \cos^{j+m}\left(\frac{\theta_0}{2}\right) \sin^{j-m}\left(\frac{\theta_0}{2}\right) e^{i(j-m)\phi_0}$$

and $\binom{n}{m} = \frac{n!}{m!(n-m)!}$. For the coherent charging scheme (i.e., $c = 1$), $\hat{\rho}_A$ becomes a coherent spin state $|\theta_0, \phi_0\rangle$ [53–57], which gives the population imbalance and the phase coherence determined by $\langle \hat{J}_z \rangle = j \cos(\theta_0)$ and $\langle \hat{J}_- \rangle = c j \sin(\theta_0) \exp(-i\phi_0)$ [57,58], respectively. Hereafter, we choose the azimuthal angle $\phi_0 = 0$ and therefore

$$v = 2j \cos(\theta_0) \sin^2(\tau), \quad \Omega = c j \sin(\theta_0) \sin(2\tau), \quad (11)$$

where $j = N_A/2$ and $c = \Omega = 0$ for the incoherent protocol.

We first consider the incoherent charging process to an initially empty battery $\hat{\rho}_B(0) = |0\rangle\langle 0|$, using $\hat{\rho}_A$ with $c = 0$ and $\theta_0 = \pi/3$. The red dashed lines of Fig. 2(a) show the probability distributions $P_n(k)$ against n for different charging times $k\tau$, where $\tau = \pi/4$ is fixed [32]. One can find that the probability distribution tends to a Gaussian as k increases. Therefore, from Eq. (6), the peak of $P_n(k)$ appears at

$$n = \bar{n}_k \approx vk + \Omega \sum_{k'=0}^{k-1} \text{Im}(\beta_{k'}^*) \sim (v + \Omega)k, \quad (12)$$

where the last result holds when $\text{Im}(\beta_k) \sim 1$ (see Appendix B). From Fig. 2(a), one can see the locations of the peaks $n \approx (v + \Omega)k$, as indicated by the vertical lines. When the peak approaches the highest level (i.e., $n \approx N_B$), the battery can be regarded as being fully charged and the

number of charging steps needed is given by [32]

$$k_{est} \approx \text{Ceiling}\left[\frac{N_B}{v + \Omega}\right], \quad (13)$$

where $\text{Ceiling}[x]$ gives the smallest integer greater than or equal to x. In Fig. 2(b), we show the mean value of the excitations $\bar{n}_k$ against the total charging time $k\tau$. As shown by the red dashed line, $\bar{n}_k$ monotonically increases from 0 to its maximal value N_B. A similar result has been observed by considering the single-qubit case of $\hat{\rho}_A$ [32].

For the single-qubit case [32], it has been shown that the number of collisions $k_{est} \approx 800$, corresponding to the total charging time $k_{est}\tau \approx 628$. For the coherent charging process (i.e., $c = 1$), it is about $k_{est} = 292$ [32] and hence the total charging time $k_{est}\tau \approx 229$, which is shorter than that of the incoherent case by 2.74 times. To understand the advantage of the coherent protocol, one can note that the number of collisions k_{est} can be reduced due to $\Omega \neq 0$ (it is maximized for $\tau = \pi/4$ and is vanishing for the incoherent case), and therefore leads to a faster charging. However, when $k > k_{est}$, the coherent protocol loses its advantage, due to a decay of $\bar{n}_k$. This is because the probability distribution $P_n(k)$ is reflected by the upper boundary ($n = N_B$) [32], which reduces $\bar{n}_k$ and hence the energy of the battery $E(k)$. Such a phenomenon also occurs for the many-particle case.

For the many-particle case, e.g., $N_A = 10$, the charging time can be further reduced for both the incoherent and the coherent protocols. As shown by Fig. 2(b), the incoherent scheme requires $k_{est}\tau \approx 63$ (the red dashed line) to fully charge the battery. For the coherent case (the solid line), the total charging time is about $k_{est}\tau \approx 23$. Indeed, the number of charging steps k_{est} is reduced by N_A times since both v and Ω are proportional to j ($= N_A/2$), as Eqs. (11) and (13). Therefore, a faster charging can be realized by using the many-particle $\hat{\rho}_A$.

In Figs. 2(c) and 2(d), we further consider the above two charging processes in the short-time limit (e.g., $\tau = 10^{-2}$). For this case, the coherent protocol always outperforms the incoherent one within the total charging time $k\tau \in [0, 70]$. For the incoherent case, both $P_n(k)$ and $\bar{n}_k$ increase very slowly (the red dashed lines). Indeed, the battery is fully charged when $k_{est}\tau \approx 4 \times 10^3$. In contrast, the coherent scheme significantly reduces the total charging time. One can see that $\bar{n}_k$ increases to its maximum at $k_{est}\tau \approx 23$, with a very small value of interaction time $\tau = 10^{-2}$. This result is somewhat counterintuitive.

To understand the above result, we derive analytical results of $\bar{n}_k$ and hence the charging power in the short-time limit (i.e., $\tau \ll 1$). According to Eqs. (7) and (8), $\bar{n}_k$ depends on β_k and also $\langle 0|\hat{\rho}_B(k)|0\rangle \approx |\langle 0|\hat{D}(k\alpha)|0\rangle|^2$, where

$$\langle 0|\hat{D}(k\alpha)|0\rangle = \sum_{l=0}^{\infty} \frac{k^l}{l!} \langle 0|(\alpha\hat{B}^\dagger - \alpha^*\hat{B})^l|0\rangle, \quad (14)$$

with $\alpha = i\tau\langle\hat{J}_-\rangle$. Performing a series expansion over $\langle 0|(\alpha\hat{B}^\dagger - \alpha^*\hat{B})^l|0\rangle$, one can see that it is vanishing for odd l (see Appendix B). As inspired by Fig. 3(a), for even $l = 2n$, we obtain $\langle 0|(\alpha\hat{B}^\dagger - \alpha^*\hat{B})^{2n}|0\rangle = (-1)^n|\alpha|^{2n}C_n$,
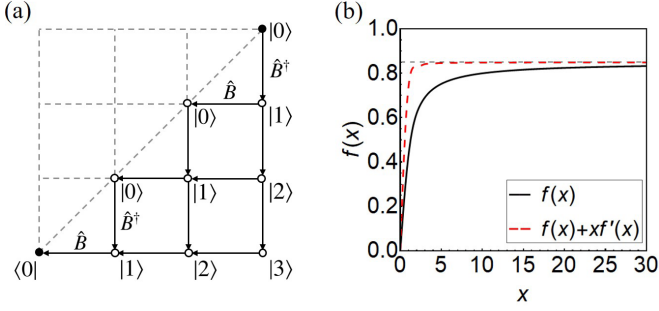
FIG. 3. (a) All possible paths for $\langle 0|(\alpha^* \hat{B} - \alpha \hat{B}^\dagger)^{2n}|0\rangle \neq 0$, with the number of paths given by the Catalan number C_n. (b) The monotonic function $f(x)$ (solid), defined by Eq. (19), and $f(x) + xf'(x)$ (red dashed). In (a), the number of paths $C_n = 5$ for $n = 3$. Horizontal line in (b): $8/(3\pi)$.

where $C_n = \frac{1}{n+1}\binom{2n}{n}$ denotes the Catalan number [59,60] and therefore

$$\langle 0|\hat{D}(k\alpha)|0\rangle = \sum_{n=0}^{\infty} \frac{(-1)^n (k|\alpha|)^{2n} C_n}{(2n)!} = \frac{J_1(2k|\alpha|)}{k|\alpha|}. \quad (15)$$

Here $J_1(x)$ denotes the first-order Bessel function of the first kind. Now Eq. (8) becomes

$$\beta_k \approx \beta_0 - \alpha \sum_{k'=0}^{k-1} \left(\frac{J_1(2k'|\alpha|)}{k'|\alpha|}\right)^2, \quad (16)$$

where $\beta_0 = \mathrm{Tr}_B[\hat{\rho}_B(0)\hat{B}] = 0$. From Eq. (7), we further obtain (see Appendix B)

$$\bar{n}_k \approx 2 \sum_{k'=0}^{k-2} (k - 1 - k') \left(\frac{J_1(2k'|\alpha|)}{k'}\right)^2, \quad (17)$$

where $\bar{n}_0 = 0$. For a large enough k (so that $k - 2 \approx k$), the sum over k' can be replaced by an integral

$$\bar{n}_k \approx 2 \int_0^k (k - k') \left(\frac{J_1(2k'|\alpha|)}{k'}\right)^2 dk' = 2xf(x), \quad (18)$$

where $x = k|\alpha| = k\tau\langle\hat{J}_-\rangle$, with $\langle\hat{J}_-\rangle = j\sin(\theta_0)$, and

$$f(x) = \frac{1}{x} \int_0^x (x - x') \left[\frac{J_1(2x')}{x'}\right]^2 dx'. \quad (19)$$

From Fig. 3(b), one can see that $f(x)$ is a monotonic function, which increases from 0 to its asymptotic value $f(\infty) = 8/(3\pi) \approx 0.85$. When $x = 30$, $f(x)$ approaches $f(\infty)$.

Note that Eqs. (17) and (18) are valid for $\hat{\rho}_B(0) = |0\rangle\langle 0|$ and $k\tau \leqslant k_{\mathrm{est}}\tau$, where the charging time per collision $\tau \ll 1$. In the short-time limit, from Eq. (13), we obtain $k_{\mathrm{est}}\tau \approx \tau\mathrm{Ceiling}[N_B/\Omega] \sim N_B/N_A$, provided $\theta_0 = \pi/2$. As depicted by Fig. 2(d), our analytical results (the circles) show a good agreement with the numerical result of $\bar{n}_k$, as long as $k\tau \leqslant k_{\mathrm{est}}\tau \approx 23$. Furthermore, Eq. (17) at $k = k_{\mathrm{est}}$ gives $\bar{n}_k \approx 0.82N_B$, which coincides quite well with the numerical result $0.87N_B$. Numerical results of $\bar{n}_k$ decrease after $k\tau \gtrsim k_{\mathrm{est}}\tau$, which cannot be predicted by our analytical result.

IV. CHARGING POWER

The performance of the battery can be quantified by the charging power

$$P = \frac{E(k) - E(0)}{kt} = g\varepsilon\left(\frac{\bar{n}_k - \bar{n}_0}{k\tau}\right), \quad (20)$$

where $E(0) = \varepsilon\bar{n}_0$ is the mean energy of the initially uncharged battery. For the fully empty battery, $\hat{\rho}_B(0) = |0\rangle\langle 0|$, we have $E(0) = \bar{n}_0 = 0$. Using Eq. (12), one can obtain an approximate upper bound of the power,

$$P \approx \frac{g\varepsilon}{\tau}(v + \Omega) = g\varepsilon N_A \frac{\sin(\tau)}{\tau} \sin(\tau + \theta_0) \leqslant g\varepsilon N_A, \quad (21)$$

where v and Ω are given in Eq. (11). The first result comes from Eq. (12) when $\mathrm{Im}(\beta_k) \sim 1$, valid for the no-boundary condition. The second inequality is a natural result of Eq. (11) with $c = 1$. One can easily find that the maximum of the power can be reached at $\theta_0 = \pi/2 - \tau$. Therefore, in the limit $\tau \to 0$ (i.e., $\theta_0 \approx \pi/2$), the power is possible to reach its upper bound $g\varepsilon N_A$.

To reach the upper bound, we now consider the coherent charging of the initially empty battery [i.e., $c = 1$ and $\hat{\rho}_B(0) = |0\rangle\langle 0|$], using an optimal atom state $|\pi/2, 0\rangle$. In the short-time limit $\tau \to 0$, Fig. 2(d) suggests a large enough number of the atom-battery interactions (i.e., $k \to \infty$, but with a finite total charging time $k\tau$). Using Eq. (18), we obtain the analytical result of the power

$$P_{\mathrm{coh}} \approx \frac{2g\varepsilon}{k\tau} xf(x) = 2g\varepsilon\langle\hat{J}_-\rangle f(x), \quad (22)$$

where $x = k\tau\langle\hat{J}_-\rangle$, with $\langle\hat{J}_-\rangle = j\sin(\theta_0)$. The optimal atom state $|\theta_0, 0\rangle$ with $\theta_0 = \pi/2$ can be obtained from the following equation:

$$0 = \frac{\partial P_{\mathrm{coh}}}{\partial \theta_0} \propto \frac{\partial x}{\partial \theta_0}\left[f(x) + x\frac{\partial f(x)}{\partial x}\right] \quad (23)$$

or, equivalently, $0 = \partial x/\partial\theta_0 \propto \partial\langle\hat{J}_-\rangle/\partial\theta_0 = j\cos(\theta_0)$, i.e., $\theta_0 = \pi/2$. With the optimal state, the charging power P_{coh} can reach its maximum at $k_{\mathrm{est}}\tau \sim N_B/N_A$, with

$$P_{\mathrm{coh,max}} \approx N_A g\varepsilon f(\infty) = \frac{8}{3\pi} N_A g\varepsilon, \quad (24)$$

where $f(\infty) = 8/(3\pi) \approx 0.85$, as shown by Fig. 3(b). In the single-particle picture, the optimal atom state can be rewritten as a direct product $|\pi/2, 0\rangle \propto (|e\rangle + |g\rangle)^{\otimes N_A}$, corresponding to all the spins pointed to the $\hat{J}_x$ axis, as depicted in Fig. 1. The coherent spin state with $\theta_0 = \pi/2$ has been prepared in the large spin system at the room temperature [48,49] and the ultracold bosonic gases in optical lattice [50–52].

The coherent charging scheme is robust to imperfections in preparing the atomic states. As shown in Fig. 4(a), one can see that P_{coh} varies smoothly with θ_0 for different values of N_A. No peak or dip at $\theta_0 \sim \pi/2$ means that the coherent scheme works well for a suboptimal atom state. When θ_0 largely departs from $\pi/2$ (e.g., $\theta_0 = \pi/8$), the squares of Fig. 4(b) show that the power $P_{\mathrm{coh,max}} \approx 0.85g\varepsilon N_A$ can almost be maintained by taking a relatively larger charging time τ, which has not been investigated in Ref. [32].
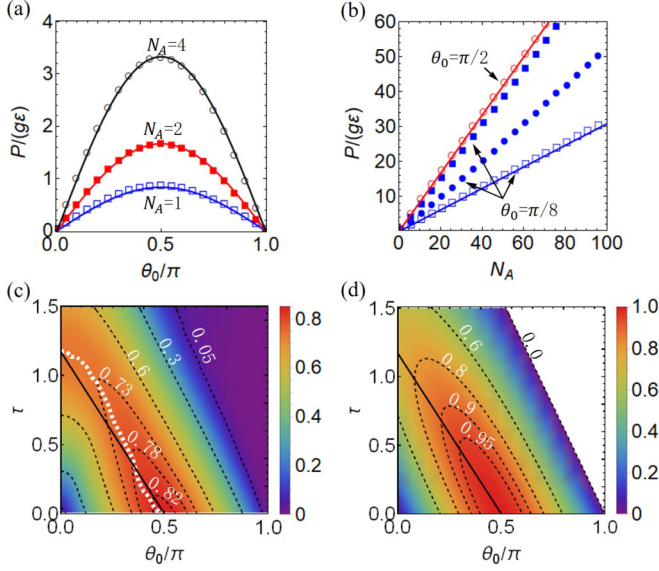
FIG. 4. (a) Scaled power $P/(g\varepsilon)$ against θ_0 for a fixed $\tau = 0.01$ and different numbers of the atoms, (b) the charging power against N_A for $\theta_0 = \pi/8$ and different values of τ, and (c) and (d) numerical and analytical results of $P/(g\varepsilon N_A)$ as functions of θ_0 and τ. All the numerical results are obtained at $k\tau = 60/N_A$. In (a): from top to bottom, $N_A = 4$ (open circles), 2 (squares), and 1 (open squares), coincident with the curves for Eq. (22). In (b): from top to bottom, $\tau = 0.88$ (squares), 0.3 (circles), and 0.01 (open squares), to comparing with the optimal result (the open circles for $\theta_0 = \pi/2$ and $\tau = 0.01$), and the curves also from Eq. (22). The white dashed line of (c): local maximum of the power at $k\tau = 60/N_A$ for $N_A = 10$ and different values of (θ_0, τ), to comparing with its analytical result $\tau = 1.17(1 - 2\theta_0/\pi)$ (solid line), obtained from the second result of Eq. (21). All for $N_B = 200$.

To confirm the above results, we consider the coherent charging to the initially empty battery [i.e., $c = 1$ and $\hat{\rho}_B(0) = |0\rangle\langle 0|$]. In Fig. 4, we choose a fixed charging time $k\tau = 60/N_A$ to calculate numerical results of $\bar{n}_k$ and hence the power P, which depend on the choices of θ_0 and τ. For given $N_A = 1$ (the open squares), 2 (the squares), and 4 (the open circles), in Fig. 4(a), we take $\tau = 0.01$ (i.e., from bottom to top, $k = 6000$, 3000, and 1500) and show the scaled power as a function of θ_0. As $\tau \ll 1$, one can see that our analytical results work well (the curves) and the maximum of the power appears at $\theta_0 = \pi/2$. When θ_0 largely departs from $\pi/2$, e.g., $\theta_0 = \pi/8$ in Fig. 4(b), we show the power as a function of N_A for $\tau = 0.01$ (the open squares), 0.3 (the circles), and 0.88 (the squares). From the squares, one can see that the optimal result $P_{\text{coh,max}}$ that is obtained for $\theta_0 = \pi/2$ and $\tau \ll 1$ (the open circles) is almost maintained by choosing a relatively larger charging time τ.

In Fig. 4(c), we take $N_A = 10$ and show the scaled power $P/(g\varepsilon N_A)$ against θ_0 and τ. When $\tau \ll 1$, the optimal atom state corresponds to $\theta_0 = \pi/2$, as expected, while for each value of $\theta_0 < \pi/2$, there exists an optimal value of the charging time τ (the white dashed line). In Fig. 4(d), we show the scaled power using the second result of Eq. (21), where the white background region indicates $P \propto \sin(\tau + \theta_0) < 0$. This is unphysical. Analytically, we show that the maximum of
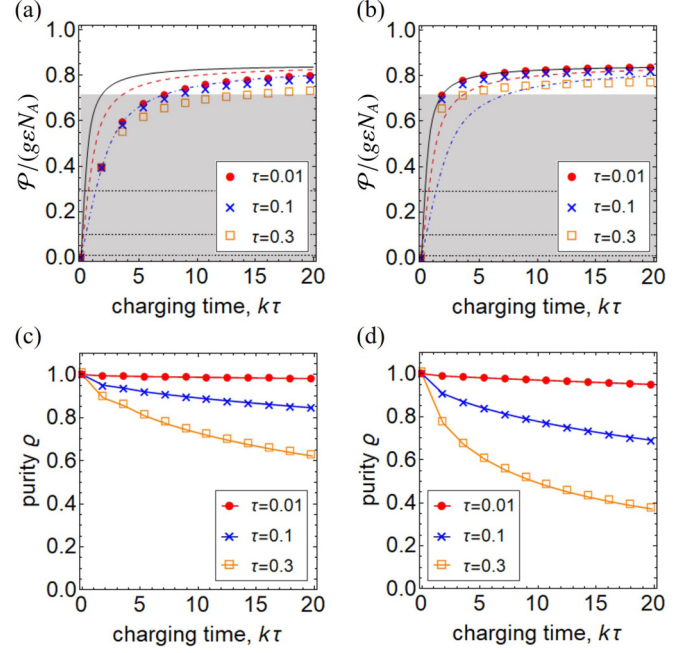

FIG. 5. With a given $\tau = 0.01$, 0.1, and 0.3, the scaled power $\mathcal{P}/(g\varepsilon N_A)$ defined by the ergotropy and the purity of $\hat{\rho}_B(k)$ for $N_A = 1$ (left panel) and 4 (right panel). The curves in (a) and (b): the scaled power $P_{\text{coh}}/(g\varepsilon N_A)$ for $N_A = 1$ (dot-dashed), 2 (dashed), and 4 (solid), obtained from Eq. (22) with $\theta_0 = \pi/2$. The horizontal lines in (a) and (b): the power of the incoherent charging scheme $P_{\text{inc}}/(g\varepsilon N_A)$ for different values of $\tau = 0.01$, 0.1, and 0.3 (from bottom to top). The top edge of the gray area: the maximum power of the incoherent charging protocol for $\tau = 1.17$, i.e., $P_{\text{inc,max}}/(g\varepsilon N_A) \simeq 0.72$. All for $N_B = 200$.

the power can be obtained for $\tau = 1.17(1 - 2\theta_0/\pi)$ (the solid line), which coincides quite well with the white dashed line of Fig. 4(c). When $\theta_0 = \pi/8$, we have $\tau = 0.88$, as depicted by the squares of Fig. 4(b). As $\theta_0 \to 0$, the maximum of the power appears at $\tau = 1.17$, which can be understood by considering the incoherent charging protocol.

For the incoherent charging case (i.e., $c = \Omega = 0$), Eq. (6) becomes $\bar{n}_k \approx kv$, and therefore

$$P_{\text{inc}} \approx 2g\varepsilon \langle \hat{J}_z \rangle \frac{\sin^2(\tau)}{\tau}, \tag{25}$$

where $\langle \hat{J}_z \rangle = j \cos(\theta_0)$. One can easily find that an optimal value of P_{inc} can be obtained for $\theta_0 = 0$, corresponding to an optimal atom state $|e\rangle^{\otimes N_A}$, as shown by Fig. 1. Furthermore, P_{inc} reaches its maximum at a finite τ, determined by

$$0 = \left.\frac{\partial P_{\text{inc}}}{\partial \tau}\right|_{\tau_0} \propto \frac{\sin^2 \tau_0}{\tau_0^2}(2\tau_0 \cot \tau_0 - 1), \tag{26}$$

or, equivalently, $\tau_0 \cot \tau_0 = 1/2$. This is a transcendental equation with one of the roots $\tau_0 \approx 1.17$ [32], which gives $P_{\text{inc,max}} \approx 0.72 g\varepsilon N_A$. Note that $P_{\text{inc,max}}$ is the achievable power attained from the incoherent charging protocol, as depicted by the top edge of the gray area in Figs. 5(a) and 5(b). Using the optimal state with $\theta_0 = 0$, Eq. (13) indicates that fully charging the battery with the incoherent protocol requires the time

$k_{est}\tau_0 \approx \tau_0 \text{Ceiling}[N_B/v] \sim 1.38 N_B/N_A$, larger than that of the coherent charging protocol ($k_{est}\tau \sim N_B/N_A$ for $\theta_0 = \pi/2$).

Comparing Eqs. (22) and (25), one can easily find that the coherent protocol depends on the atomic coherence $\langle \hat{J}_- \rangle$ and the power varies with the time $x = k\tau \langle \hat{J}_- \rangle$. For the incoherent one, however, the power is a function of τ, independent on the atomic coherence. Our analytical results show that the advantages of the coherent protocol in the charging time and that of the charging power *uniquely* arise from the phase coherence of the atoms. For the coherent spin state with $\theta_0 = \pi/2$, the coherence becomes maximum and the charging power $P_{coh,max} \approx 0.85 g\varepsilon N_A$ can be obtained for the charging time $\tau \to 0$, which significantly reduces the role of noise during each charging step. Furthermore, with a finite total charging time $k_{est}\tau \sim N_B/N_A$, one can reduce the number of charging steps k_{est} by using large N_A, which is inaccessible from Ref. [32].

Finally, it should be mentioned that the useful energy of $\hat{\rho}_B(k)$ that can be extracted is given by the so-called ergotropy [45]:

$$\mathcal{E}_B(k) = E(k) - \text{Tr}_B[\hat{\sigma}_B(k)\hat{H}_B], \qquad (27)$$

where $\hat{H}_B = \varepsilon\hat{n}$ is the free Hamiltonian of the battery and $\hat{\sigma}_B(k) = \sum_n r_n |n\rangle\langle n|$, known as the passive state [61,62], is dependent on the eigenvalues of $\hat{\rho}_B(k)$ that are arranged in descending order (i.e., $r_n \leqslant r_{n+1}$). In terms of the ergotropy, one can define another kind of power:

$$\mathcal{P} = \frac{\mathcal{E}_B(k)}{kt} = g\varepsilon\left(\frac{\bar{n}_k - \text{Tr}_B[\hat{\sigma}_B(k)\hat{n}]}{k\tau}\right). \qquad (28)$$

Note that $\mathcal{E}_B(k) \leqslant E(k)$ and hence $\mathcal{P} \leqslant P$, where the equality holds for a pure state of $\hat{\rho}_B(k)$. As shown in Figs. 5(a) and 5(b), we show numerical results of $\mathcal{P}$ for $N_A = 1$ and 4 by taking fixed charging times $\tau = 0.3$ (the open squares), 0.1 (the crosses), and 0.01 (the circles). With the short-time case (i.e., $\tau = 0.01$), one can see that the circles show a good agreement with the analytical results of Eq. (22). To understand it, we calculate the purity of the battery state $\varrho = \text{Tr}_B[\hat{\rho}_B^2(k)]$, where $\varrho = 1$ for a pure state and $\varrho < 1$ for a mixed state. The purity ϱ has also been investigated in the ultrastrong atom-field interaction [33] to show the pure state of the battery. As depicted in Figs. 5(c) and 5(d), one can see $\varrho \approx 1$ for $\tau = 0.01$, indicating a nearly pure state of $\hat{\rho}_B(k)$, which in turn gives $\mathcal{E}_B(k) \approx E(k)$ and hence $\mathcal{P} \approx P$. For a larger charging time $\tau = 0.3$, the battery state becomes more and more mixed, leading to a departure of $\mathcal{P}$ from P.

V. DISCUSSION AND CONCLUSION

We have generalized the repeated atom-battery interaction model (i.e., the so-called collisional battery [32]) from the spin-1/2 charger to the case of a large spin $j = N_A/2$, where the battery is modeled by the energy ladder with a finite number of levels $N_B + 1$. Assuming little population over the battery states $|0\rangle$ and $|N_B\rangle$ (corresponding to the no-boundary problem), we first derive a recursion relation of the averaged excitation that is stored in the battery [see Eq. (6) and Appendix A], which is independent from any specific form of the atom state, and also free from the initial state of $\hat{\rho}_B(0)$. Similar to the single-atom case (i.e., the number of

two-level atoms $N_A = 1$) [32], the incoherent and the coherent charging protocols have been investigated by considering the atoms prepared in a mixed state and a coherent spin state $|\theta_0, \phi_0\rangle$, respectively. For the coherent protocol, the atomic coherence $\langle \hat{J}_- \rangle = j \sin(\theta_0) \neq 0$, leading to a reduced charging time $k_{est}\tau \sim N_B/N_A$, where k_{est} is the number of collisions for the battery being fully charged and τ is the charging time per collision.

Next, we focus on the coherent charging process over the initially empty battery in the short-time limit (i.e., $\tau \to 0$). Analytical results of the average number of excitations [see Eqs. (17) and (18)] have been derived, which are related to the first-order Bessel function of the first kind. Our results show that the maximum of the charging power $P_{coh,max} \approx 0.85 g\varepsilon N_A$ can be obtained by using the optimal coherent state $|\theta_0, 0\rangle$ with $\theta_0 = \pi/2$. With a fixed charging time $k\tau = 60/N_A$, we calculate the power against θ_0 and τ. For $\tau \ll 1$, the optimal state corresponds to $\theta_0 = \pi/2$. When the atom state is imperfect and $\theta_0 < \pi/2$, the power almost follows $P_{coh,max}$, provided that a relatively larger value of $\tau \sim 1.17(1 - 2\theta_0/\pi)$ is adopted. As $\theta_0 \to 0$, the maximum power $P_{inc,max} \approx 0.72 g\varepsilon N_A$ appears at $\tau = 1.17$, coincident with the single-atom case [32]. Finally, another kind of charging power has been investigated in terms of the so-called ergotropy. In the short-time limit, we find that numerical results of the power show good agreement with its analytical result, due to a nearly pure state of the battery in the early charging steps (i.e., $k \lesssim 0.1 k_{est}$).

In summary, we have generalized the collision model to investigate coherent charging of a single quantum battery by repeated interactions with finite N_A two-level atoms. Analytical results of the average number of excitations and hence the charging power have been derived in the short-time limit. Using an optimal coherent spin state with $\theta_0 = \pi/2$, we obtain the total charging time $k_{est}\tau \sim N_B/N_A$ and the achievable charging power $0.85 g\varepsilon N_A$, where N_B is the number of the levels of the battery and $g\varepsilon N_A$ is the upper bound of the charging power. The faster charging time and the increased amount of the power in comparison with the incoherent charging protocol uniquely arise from the phase coherence of the atoms. With a fixed charging time $k\tau$, we investigate the optimal choices of the initial atom state θ_0 and the charging time per collision τ. When θ_0 largely departs from its optimal value $\pi/2$, the achievable charging power can be almost maintained by choosing a relatively large value of $\tau \sim 1.17(1 - 2\theta_0/\pi)$. Finally, we show that the charging power defined by the ergotropy almost follows its analytical result, since the purity of the battery is almost equal to 1, indicating a nearly pure state of the battery in the short-time limit. The above results rely on the assumption that the atom states are identical for all the collisions. Indeed, it is interesting to investigate the dependence of the atom states on the charging steps (e.g., a defect state randomly appeared at one of the steps).

APPENDIX A: DETAILS OF EQS. (4) AND (6)

In the short-time limit, we have $\hat{U}_\tau \approx 1 - i\tau(\hat{J}_+\hat{B} + \hat{J}_-\hat{B}^\dagger)$ and therefore Eq. (3) becomes

$$\hat{\rho}_B(k) = \text{Tr}_A[\hat{U}_\tau \hat{\rho}_B(k-1) \otimes \rho_A \hat{U}_\tau^\dagger]$$
$$\approx \hat{\rho}_B(k-1) + [(\alpha^*\hat{B} - \alpha\hat{B}^\dagger)\hat{\rho}_B(k-1) + \text{H.c.}]$$
$$\approx (1 + \alpha^*\hat{B} - \alpha\hat{B}^\dagger)\hat{\rho}_B(k-1)(1 - \alpha^*\hat{B} + \alpha\hat{B}^\dagger),$$

with $\alpha = i\tau\langle\hat{J}_-\rangle$ and $\langle(\cdots)\rangle = \text{Tr}_A[\hat{\rho}_A(\cdots)]$. Iterating the above equation for k times, we obtain

$$\hat{\rho}_B(k) \approx (1 + \alpha^*\hat{B} - \alpha\hat{B}^\dagger)^k \rho_B(0)(1 - \alpha^*\hat{B} + \alpha\hat{B}^\dagger)^k$$
$$\approx \hat{D}^\dagger(k\alpha)\hat{\rho}_B(0)\hat{D}(k\alpha), \quad (A1)$$

as Eq. (4) in the main text.

Next, we calculate the mean number of the excitations

$$\bar{n}_k = \text{Tr}_B[\hat{\rho}_B(k)\hat{n}]$$
$$= \text{Tr}[\hat{U}_\tau\hat{\rho}_B(k-1) \otimes \hat{\rho}_A \hat{U}_\tau^\dagger \hat{n}]$$
$$= \text{Tr}[\hat{\rho}_B(k-1) \otimes \hat{\rho}_A \hat{U}_\tau^\dagger \hat{n}\hat{U}_\tau], \quad (A2)$$

where, in the second step, we have used Eq. (3) in the main text and $\hat{n} = \sum_{n=0}^{N_B} n|n\rangle\langle n|$, satisfying

$$[\hat{B}, \hat{n}] = \hat{B}, \quad [\hat{B}^\dagger, \hat{n}] = -\hat{B}^\dagger. \quad (A3)$$

Therefore, one can expand the term $\hat{U}_\tau^\dagger \hat{n}\hat{U}_\tau$ using the Baker-Campbell-Hausdorff formula,

$$\hat{U}_\tau^\dagger \hat{n}\hat{U}_\tau = e^{i\tau(\hat{J}_+\hat{B}+\hat{J}_-\hat{B}^\dagger)} \hat{n} \, e^{-i\tau(\hat{J}_+\hat{B}+\hat{J}_-\hat{B}^\dagger)} = \sum_{k=0}^\infty \frac{1}{k!}\hat{C}_k, \quad (A4)$$

where $\hat{C}_{k+1} = i\tau[\hat{J}_+\hat{B} + \hat{J}_-\hat{B}^\dagger, \hat{C}_k]$. Starting from $\hat{C}_0 = \hat{n}$, we obtain

$$\hat{C}_1 = i\tau[\hat{J}_+\hat{B} + \hat{J}_-\hat{B}^\dagger, \hat{C}_0]$$
$$= i\tau(\hat{J}_+[\hat{B}, \hat{n}] + \hat{J}_-[\hat{B}^\dagger, \hat{n}])$$
$$= i\tau(\hat{J}_+\hat{B} - \hat{J}_-\hat{B}^\dagger), \quad (A5)$$

where we have used Eq. (A3). Next, we obtain

$$\hat{C}_2 = i\tau[\hat{J}_+\hat{B} + \hat{J}_-\hat{B}^\dagger, \hat{C}_1] = 2\tau^2[\hat{J}_+\hat{B}, \hat{J}_-\hat{B}^\dagger]$$
$$= 2\tau^2(\hat{J}_+[\hat{B}, \hat{J}_-\hat{B}^\dagger] + [\hat{J}_+, \hat{J}_-\hat{B}^\dagger]\hat{B}) \approx (2\tau)^2\hat{J}_z, \quad (A6)$$

where we have used the commutation relation $[\hat{J}_+, \hat{J}_-] = 2\hat{J}_z$, as well as $[\hat{B}, \hat{B}^\dagger] \approx 0$ and $\hat{B}^\dagger\hat{B} = 1 - |0\rangle\langle 0| \approx 1$, valid for the no-boundary condition (i.e., the occupations of $|0\rangle$ and $|N_B\rangle$ being vanishing). Similarly, we obtain

$$\hat{C}_3 = i\tau[\hat{J}_+\hat{B} + \hat{J}_-\hat{B}^\dagger, \hat{C}_2] = -4i\tau^3(\hat{J}_+\hat{B} - \hat{J}_-\hat{B}^\dagger),$$
$$\hat{C}_4 = i\tau[\hat{J}_+\hat{B} + \hat{J}_-\hat{B}^\dagger, \hat{C}_3] \approx -(2\tau)^4\hat{J}_z,$$

and so on. Finally, one can easily obtain

$$\hat{U}_\tau^\dagger \hat{n}\hat{U}_\tau \approx \hat{n} + \frac{(\hat{J}_-\hat{B}^\dagger - \hat{J}_+\hat{B})}{2i} \sum_{k=0}^\infty \frac{(-1)^k}{(2k+1)!}(2\tau)^{2k+1}$$

$$+ \hat{J}_z \sum_{k=0}^\infty \frac{(-1)^k}{(2k+2)!}(2\tau)^{2k+2}$$

$$= \hat{n} + \sin(2\tau)\frac{(\hat{J}_-\hat{B}^\dagger - \hat{J}_+\hat{B})}{2i} + 2\sin^2(\tau)\hat{J}_z.$$

Therefore, Eq. (A2) becomes

$$\bar{n}_k \approx \bar{n}_{k-1} + 2\sin^2(\tau)\langle\hat{J}_z\rangle + \sin(2\tau)\text{Im}(\langle\hat{J}_-\rangle\beta_{k-1}^*), \quad (A7)$$

as Eq. (6) in the main text, where $\beta_k = \text{Tr}_B[\hat{\rho}_B(k)\hat{B}]$.

APPENDIX B: DETAILS OF EQS. (8) AND (17)

First, we calculate β_k for the battery state $\hat{\rho}_B(k)$ defined by Eq. (3) in the main text,

$$\beta_k = \text{Tr}_B[\hat{\rho}_B(k)\hat{B}]$$
$$= \text{Tr}[\hat{U}_\tau\hat{\rho}_B(k-1) \otimes \hat{\rho}_A \hat{U}_\tau^\dagger \hat{B}]$$
$$= \text{Tr}[\hat{\rho}_B(k-1) \otimes \hat{\rho}_A \hat{U}_\tau^\dagger \hat{B}\hat{U}_\tau]. \quad (B1)$$

Similar to Eq. (A4), we deal with the term

$$\hat{U}_\tau^\dagger \hat{B}\hat{U}_\tau = e^{i\tau(\hat{J}_+\hat{B}+\hat{J}_-\hat{B}^\dagger)} \hat{B} \, e^{-i\tau(\hat{J}_+\hat{B}+\hat{J}_-\hat{B}^\dagger)} = \sum_{k=0}^\infty \frac{1}{k!}\hat{D}_k, \quad (B2)$$

where $\hat{D}_{k+1} = i\tau[\hat{J}_+\hat{B} + \hat{J}_-\hat{B}^\dagger, \hat{D}_k]$, with $\hat{D}_0 = \hat{B}$. In the short-time limit, the first-order expansion is enough, i.e.,

$$\hat{U}_\tau^\dagger \hat{B}\hat{U}_\tau \approx \hat{B} + \hat{D}_1, \quad (B3)$$

where

$$\hat{D}_1 = i\tau[\hat{J}_+\hat{B} + \hat{J}_-\hat{B}^\dagger, \hat{D}_0]$$
$$= i\tau\hat{J}_-[\hat{B}^\dagger, \hat{B}] = i\tau\hat{J}_-(|N_B\rangle\langle N_B| - |0\rangle\langle 0|). \quad (B4)$$

Therefore, we obtain

$$\beta_k \approx \text{Tr}_B[\hat{\rho}_B(k-1)\hat{B} + \alpha\hat{\rho}_B(k-1)\hat{D}_1]$$
$$= \beta_{k-1} + \alpha\text{Tr}_B[\hat{\rho}_B(k-1)(|N_B\rangle\langle N_B| - |0\rangle\langle 0|)]$$
$$= \beta_{k-1} + \alpha[\langle N_B|\hat{\rho}_B(k-1)|N_B\rangle - \langle 0|\hat{\rho}_B(k-1)|0\rangle]$$
$$= \beta_0 + \sum_{k'=0}^{k-1} \alpha[\langle N_B|\hat{\rho}_B(k')|N_B\rangle - \langle 0|\hat{\rho}_B(k')|0\rangle], \quad (B5)$$

where the last second result has been iterated for k times. With the no-boundary condition, we simply obtain $\beta_k \approx \beta_0$; neglecting only the upper boundary $|N_B\rangle$, we obtain Eqs. (8) and (16) in the main text, where the lower boundary $|0\rangle$ has been taken into account.

Next, we analyze β_k for an arbitrary state $\hat{\rho}_B(k) = \sum_i p_i|\psi_B^{(i)}\rangle\langle\psi_B^{(i)}|$, where $|\psi_B^{(i)}\rangle = \sum_{n=0}^{N_B} c_n^{(i)}|n\rangle$ and $\sum_i p_i = 1$, which gives the Cauchy-Schwartz inequality:

$$|\beta_k| = \left|\sum_{n=0}^{N_B} \langle n|\hat{\rho}_B(k)\hat{B}|n\rangle\right| \leqslant \sum_i p_i \left|\sum_{n=1}^{N_B} c_n^{(i)} c_{n-1}^{(i)*}\right|$$

$$\leqslant \sum_i p_i \sqrt{\sum_{n=1}^{N_B} |c_n^{(i)}|^2 \sum_{n'=1}^{N_B} |c_{n'-1}^{(i)}|^2}$$

$$= \sum_i p_i \sqrt{(1 - |c_0^{(i)}|^2)(1 - |c_{N_B}^{(i)}|^2)}$$

$$\leqslant 1.$$

Note that the equality in the second step holds for $c_n^{(i)} c_{n-1}^{(i)*} \in \mathbb{R}$. The following two equalities hold for $c_n^{(i)} = c_{n-1}^{(i)*}$ and $c_0^{(i)} = c_{N_B}^{(i)} = 0$, respectively. Therefore, it is easy to obtain $|\beta_k| \in [0, 1)$, which has been used in Eq. (12).

Finally, we calculate Eq. (A2) in the short-time limit to derive Eq. (17) in the main text. Using $\hat{U}_\tau^\dagger \hat{n} \hat{U}_\tau \approx \hat{n} + \hat{C}_1 = \hat{n} + i\tau(\hat{J}_+ \hat{B} - \hat{J}_- \hat{B}^\dagger)$, we obtain

$$\bar{n}_k \approx \mathrm{Tr}_B[\hat{\rho}_B(k-1)\hat{n} - \hat{\rho}_B(k-1)(\alpha\hat{B}^\dagger + \alpha^*\hat{B})]$$

$$= \bar{n}_{k-1} - (\alpha\beta_{k-1}^* + \alpha^*\beta_{k-1}), \tag{B6}$$

as Eq. (7) in the main text. Iterating the above equation for k times, we further obtain

$$\bar{n}_k \approx \bar{n}_0 - \sum_{k'=0}^{k-1}(\alpha\beta_{k'}^* + \alpha^*\beta_{k'}), \tag{B7}$$

where $\bar{n}_0 = 0$ for $\hat{\rho}_B(0) = |0\rangle\langle 0|$, and β_k depends on the terms $\langle 0|(\alpha\hat{B}^\dagger - \alpha^*\hat{B})^l|0\rangle$, as Eq. (14) in the main text. For odd l, e.g., $l = 1$, it is easy to see $\langle 0|(\alpha\hat{B}^\dagger - \alpha^*\hat{B})|0\rangle = \alpha\langle 0|1\rangle = 0$. As a result, we only consider even $l = 2n$, e.g., $n = 1$,

$$\langle 0|(\alpha\hat{B}^\dagger - \alpha^*\hat{B})^2|0\rangle$$

$$= \langle 0|[(\alpha\hat{B}^\dagger)^2 + (-\alpha^*\hat{B})^2 - |\alpha|^2\hat{B}^\dagger\hat{B} - |\alpha|^2\hat{B}\hat{B}^\dagger]|0\rangle$$

$$= -|\alpha|^2\langle 0|[\hat{B}^\dagger\hat{B} + \hat{B}\hat{B}^\dagger]|0\rangle = -|\alpha|^2\langle 0|\hat{B}\hat{B}^\dagger|0\rangle$$

$$= -|\alpha|^2.$$

To obtain $\langle 0|(\alpha\hat{B}^\dagger - \alpha^*\hat{B})^{2n}|0\rangle \neq 0$ requires the numbers of $\hat{B}$ and $\hat{B}^\dagger$ to be equal. Furthermore, the ordering over the

ladder operators $\hat{B}$ and $\hat{B}^\dagger$ corresponds to the evolution paths from the "initial" state $|0\rangle$ to the "final" state $|0\rangle$, as depicted by Fig. 3(a), where each path gives the same value $(-|\alpha|^2)^n$ and the number of all possible paths is given by the Catalan number $C_n = \frac{1}{n+1}\binom{2n}{n}$. Therefore, we obtain

$$\langle 0|(\alpha\hat{B}^\dagger - \alpha^*\hat{B})^{2n}|0\rangle = (-1)^n|\alpha|^{2n}C_n. \tag{B8}$$

Substituting it into Eq. (14), we obtain Eqs. (15) and (16) in the main text and therefore

$$\bar{n}_k \approx 2\sum_{k'=0}^{k-1}\sum_{l=0}^{k'-1}\left(\frac{J_1(2l|\alpha|)}{l}\right)^2$$

$$= 2\sum_{k'=1}^{k-1}\sum_{l=0}^{k'-1}\left(\frac{J_1(2l|\alpha|)}{l}\right)^2$$

$$= 2\sum_{l=0}^{k-2}\sum_{k'=l+1}^{k-1}\left(\frac{J_1(2l|\alpha|)}{l}\right)^2$$

$$= 2\sum_{l=0}^{k-2}(k-1-l)\left(\frac{J_1(2l|\alpha|)}{l}\right)^2, \tag{B9}$$

where, in the last two steps, we have interchanged the order of summation $\sum_{k'=1}^{k-1}\sum_{l=0}^{k'-1}(\cdots) = \sum_{l=0}^{k-2}\sum_{k'=l+1}^{k-1}(\cdots)$ and note the inner sum $\sum_{k'=l+1}^{k-1}(\cdots) = (k-l-1)(\cdots)$.

---

[1] M. Horodecki and J. Oppenheim, Nat. Commun. **4**, 2059 (2013).

[2] W. Niedenzu, V. Mukherjee, A. Ghosh, A. G. Kofman, and G. Kurizki, Nat. Commun. **9**, 165 (2018).

[3] J. Goold, M. Huber, A. Riera, L. del Rio, and P. Skrzypczyk, J. Phys. A: Math. Theor. **49**, 143001 (2016).

[4] S. Vinjanampathy and J. Anders, Contemp. Phys. **57**, 545 (2016).

[5] F. Campaioli, F. A. Pollock, and S. Vinjanampathy, *Thermodynamics in the Quantum Regime, Fundamental Aspects and New Directions* (Springer, Cham, Switzerland, 2018).

[6] R. Alicki and M. Fannes, Phys. Rev. E **87**, 042123 (2013).

[7] K. V. Hovhannisyan, M. Perarnau-Llobet, M. Huber, and A. Acín, Phys. Rev. Lett. **111**, 240401 (2013).

[8] F. Barra, Phys. Rev. Lett. **122**, 210601 (2019).

[9] S. Bhattacharjee and A. Dutta, Eur. Phys. J. B **94**, 239 (2021).

[10] G. M. Andolina, M. Keck, A. Mari, V. Giovannetti, and M. Polini, Phys. Rev. B **99**, 205437 (2019).

[11] Y.-Y. Zhang, T.-R. Yang, L. Fu, and X. Wang, Phys. Rev. E **99**, 052106 (2019).

[12] L. Peng, W.-B. He, S. Chesi, H.-Q. Lin, and X.-W. Guan, Phys. Rev. A **103**, 052220 (2021).

[13] T. P. Le, J. Levinsen, K. Modi, M. M. Parish, and F. A. Pollock, Phys. Rev. A **97**, 022106 (2018).

[14] S. Julià-Farré, T. Salamon, A. Riera, M. N. Bera, and M. Lewenstein, Phys. Rev. Res. **2**, 023113 (2020).

[15] F. Zhao, F.-Q. Dou, and Q. Zhao, Phys. Rev. A **103**, 033715 (2021).

[16] A. Levy, L. Diósi, and R. Kosloff, Phys. Rev. A **93**, 052119 (2016).

[17] S. Seah, S. Nimmrichter, and V. Scarani, New J. Phys. **20**, 043045 (2018).

[18] F. H. Kamin, F. T. Tabesh, S. Salimi, and A. C. Santos, Phys. Rev. E **102**, 052109 (2020).

[19] F. C. Binder, S. Vinjanampathy, K. Modi, and J. Goold, New J. Phys. **17**, 075015 (2015).

[20] F. Campaioli, F. A. Pollock, F. C. Binder, L. Céleri, J. Goold, S. Vinjanampathy, and K. Modi, Phys. Rev. Lett. **118**, 150601 (2017).

[21] A. C. Santos, A. Saguia, and M. S. Sarandy, Phys. Rev. E **101**, 062114 (2020).

[22] D. Rossini, G. M. Andolina, D. Rosa, M. Carrega, and M. Polini, Phys. Rev. Lett. **125**, 236402 (2020).

[23] J.-Y. Gyhm, D. Šafránek, and D. Rosa, Phys. Rev. Lett. **128**, 140501 (2022).

[24] D. Ferraro, M. Campisi, G. M. Andolina, V. Pellegrini, and M. Polini, Phys. Rev. Lett. **120**, 117702 (2018).

[25] G. M. Andolina, D. Farina, A. Mari, V. Pellegrini, V. Giovannetti, and M. Polini, Phys. Rev. B **98**, 205423 (2018).

[26] G. M. Andolina, M. Keck, A. Mari, M. Campisi, V. Giovannetti, and M. Polini, Phys. Rev. Lett. **122**, 047702 (2019).

[27] J. Monsel, M. Fellous-Asiani, B. Huard, and A. Auffèves, Phys. Rev. Lett. **124**, 130601 (2020).

[28] J. Q. Quach, K. E. McGhee, L. Ganzer, D. M. Rouse, B. W. Lovett, E. M. Gauger, J. Keeling, G. Cerullo, D. G. Lidzey, and T. Virgili, Sci. Adv. **8**, eabk3160 (2022).

[29] C.-K. Hu, J. Qiu, P. J. P. Souza, J. Yuan, Y. Zhou, L. Zhang, J. Chu, X. Pan, L. Hu, J. Li, Y. Xu, Y. Zhong, S. Liu, F. Yan, D. Tan, R. Bachelard, C. J. Villas-Boas, A. C. Santos, and D. Yu, Quantum Sci. Technol. **7**, 045018 (2022).

[30] I. Maillette de Buy Wenniger, S. E. Thomas, M. Maffei, S. C. Wein, M. Pont, A. Harouri, A. Lemaitre, I. Sagnes, N. Somaschi, A. Auffèves, and P. Senellart, arXiv:2202.01109.

[31] G. Gemme, M. Grossi, D. Ferraro, S. Vallecorsa, and M. Sassetti, Batteries **8**, 43 (2022).

[32] S. Seah, M. Perarnau-Llobet, G. Haack, N. Brunner, and S. Nimmrichter, Phys. Rev. Lett. **127**, 100601 (2021).

[33] V. Shaghaghi, V. Singh, G. Benenti, and D. Rosa, Quantum Sci. Technol. **7**, 04LT01 (2022).

[34] R. Salvia, M. Perarnau-Llobet, G. Haack, N. Brunner, and S. Nimmrichter, arXiv:2205.00026.

[35] J. Rau, Phys. Rev. **129**, 1880 (1963).

[36] C. M. Caves and G. J. Milburn, Phys. Rev. A **36**, 5543 (1987).

[37] T. A. Brun, Am. J. Phys. **70**, 719 (2002).

[38] F. Ciccarello, S. Lorenzo, V. Giovannetti, and G. M. Palma, Phys. Rep. **954**, 1 (2022).

[39] F. Ciccarello, G. M. Palma, and V. Giovannetti, Phys. Rev. A **87**, 040103(R) (2013).

[40] V. Scarani, M. Ziman, P. Štelmachovič, N. Gisin, and V. Bužek, Phys. Rev. Lett. **88**, 097905 (2002).

[41] P. Strasberg, G. Schaller, T. Brandes, and M. Esposito, Phys. Rev. X **7**, 021003 (2017).

[42] F. Ciccarello, Quantum Meas. Quantum Metrol. **4**, 53 (2017).

[43] N. Altamirano, P. Corona-Ugalde, R. B. Mann, and M. Zych, New J. Phys. **19**, 013035 (2017).

[44] M. T. Mitchison, J. Goold, and J. Prior, Quantum **5**, 500 (2021).

[45] A. E. Allahverdyan, R. Balian, and T. M. Nieuwenhuizen, Europhys. Lett. **67**, 565 (2004).

[46] N. Brunner, N. Linden, S. Popescu, and P. Skrzypczyk, Phys. Rev. E **85**, 051117 (2012).

[47] P. Erker, M. T. Mitchison, R. Silva, M. P. Woods, N. Brunner, and M. Huber, Phys. Rev. X **7**, 031022 (2017).

[48] T. Fernholz, H. Krauter, K. Jensen, J. F. Sherson, A. S. Sørensen, and E. S. Polzik, Phys. Rev. Lett. **101**, 073601 (2008).

[49] R. Auccaise, A. G. Araujo-Ferreira, R. S. Sarthour, I. S. Oliveira, T. J. Bonagamba, and I. Roditi, Phys. Rev. Lett. **114**, 043604 (2015).

[50] A. Widera, S. Trotzky, P. Cheinet, S. Fölling, F. Gerbier, I. Bloch, V. Gritsev, M. D. Lukin, and E. Demler, Phys. Rev. Lett. **100**, 140401 (2008).

[51] M. F. Riedel, P. Böhi, Y. Li, T. W. Hänsch, A. Sinatra, and P. Treutlein, Nature (London) **464**, 1170 (2010).

[52] E. Pedrozo-Peñafiel, S. Colombo, C. Shu, A. F. Adiyatullin, Z. Li, E. Mendez, B. Braverman, A. Kawasaki, D. Akamatsu, Y. Xiao, and V. Vuletić, Nature (London) **588**, 414 (2020).

[53] J. M. Radcliffe, J. Phys. A: Gen. Phys. **4**, 313 (1971).

[54] F. T. Arecchi, E. Courtens, R. Gilmore, and H. Thomas, Phys. Rev. A **6**, 2211 (1972).

[55] W.-M. Zhang, D. H. Feng, and R. Gilmore, Rev. Mod. Phys. **62**, 867 (1990).

[56] M. Kitagawa and M. Ueda, Phys. Rev. A **47**, 5138 (1993).

[57] G. R. Jin, Y. C. Liu, and W. M. Liu, New J. Phys. **11**, 073049 (2009).

[58] C. G. Ji, Y. C. Liu, and G. R. Jin, Quantum Inf. Comput. **13**, 0266 (2013).

[59] P. Hilton and J. Pedersen, Math. Intell. **13**, 64 (1991).

[60] R. P. Stanley, *Catalan Numbers* (Cambridge University Press, Cambridge, UK, 2015).

[61] W. Pusz and S. L. Woronowicz, Commun. Math. Phys. **58**, 273 (1978).

[62] A. Lenard, J. Stat. Phys. **19**, 575 (1978).